ELSEVIER

Materials Science and Engineering A 487 (2008) 405–409

MATERIALS SCIENCE & ENGINEERING A

www.elsevier.com/locate/msea

Static and dynamic mechanical properties of infiltrated B_4C–Si composites

S. Hayun [a], D. Rittel [b], N. Frage [a,*], M.P. Dariel [a]

[a] *Department of Materials Engineering, Ben-Gurion University of the Negev, P.O. Box 653, Beer-Sheva 84105, Israel*
[b] *Department of Mechanical Engineering, Technion, Haifa 32000, Israel*

Received 31 July 2007; received in revised form 9 October 2007; accepted 21 November 2007

Abstract

The present paper is concerned with the static and the dynamic mechanical properties at strain-rates up to $10^3\ s^{-1}$, of ceramic composites based on porous B_4C infiltrated with molten Si. The static mechanical properties of the infiltrated composites depend on the amount of the residual silicon. The Young's modulus and the hardness increase, while the flexural strength and K_{1C} decrease with decreasing fraction of residual silicon. The dynamic strength and the initiation fracture toughness K_{1D} have significantly higher values than the corresponding static properties, and are insensitive to both the residual silicon fraction and the strain-rate up to $\dot{\varepsilon} = 10^3\ s^{-1}$.

Keywords: Boron carbide; Si-infiltrated; Mechanical properties; Dynamic properties; Microstructure; Fractography

1. Introduction

Boron carbide displays elevated hardness values which combined with its low specific weight make it appropriate for lightweight armor applications. Fully dense boron carbide parts can be manufactured only by hot pressing above 2200 °C, in the presence of sintering additives [1]. An alternative way for fabricating fully dense boron carbide-based composites is the so-called "reaction bonding" process [2,3]. According to this approach, a cold-compacted mixture of boron carbide and free carbon is infiltrated with liquid silicon. The necessity of adding free carbon to the boron carbide and the presence of residual silicon, within the infiltrated composites after the reaction bonding process, are drawbacks associated with this approach. Residual silicon lowers the mechanical properties of the composite [3,4]. In order to alleviate these drawbacks, it was suggested to infiltrate partially sintered boron carbide preforms with molten silicon. Molten silicon in contact with boron carbide creates silicon carbide by reacting with the carbon component of the carbide matrix [5]. This approach is a variant of the conventional reaction infiltration process; it adds an additional step, namely the pre-infiltration sintering of the matrix to form porous carbide, but eliminates the necessity of adding free carbon and yields a product with greatly reduced free silicon. Since hot pressed boron carbide and boron carbide composites are excellent candidates for light armor applications their behavior under dynamic loading is a relevant issue. The available information regarding dynamic behavior based on boron carbide materials mostly relates to hot pressed samples at strain-rates between 10^5 and $10^6\ s^{-1}$ [6–9]. Results regarding the dynamic behavior at lower strain-rates are scarce. Chhabildas et al. [10] investigated the dynamic response of hot pressed boron carbide under loading at strain-rate of 10^4–$10^5\ s^{-1}$, Palfey et al. [11] reported results on boron carbide–aluminum composites at strain-rates of $10^3\ s^{-1}$. No information is available in the open literature regarding the dynamic response of the boron carbide- silicon composites. The present study addresses the dynamic properties of these materials at strain-rates up to $10^3\ s^{-1}$ as well as its failure mechanisms.

2. Experimental procedure

2.1. Sample preparation

Boron carbide (Starck, Grade HS) powder was compacted at 10 MPa and sintered at 2000 and 2100 °C for 30 min in

* Corresponding author. Tel.: +972 8 6471468; fax: +972 8 6489441.
E-mail address: nfrage@bgu.ac.il (N. Frage).

0921-5093/$ – see front matter © 2007 Elsevier B.V. All rights reserved.
doi:10.1016/j.msea.2007.11.062

order to obtain preforms with 30 and 20 vol.% of total porosity respectively. The preforms were infiltrated with molten silicon at 1480 °C in a vacuum of $\sim 10^{-4}$ Torr for 20 min. Preforms with 20 and 30 vol.% porosity are denoted as S20 and S30, respectively. The ground and polished samples for the dynamic testing were typically 7 mm diameter and 3.5 mm thick. Bars $45 \times 4 \times 6$ mm and $22 \times 4 \times 6$ mm were used for fracture and three point bending tests, respectively. As fatigue pre-cracking is extremely difficult for these materials, sharp notches were introduced using a 0.2 mm thick diamond saw. It is believed that while the sharp notch is not fully equivalent to a sharp crack, the error is systematic so that the observed trends can be considered as representative.

2.2. Microstructural investigation

The microstructure of the samples was studied by scanning electron microscopy (SEM, JEOL-35) combined with an energy-dispersive spectrometer (EDS). The samples for SEM characterization were prepared using a standard metallographic procedure that included a last stage of polishing with 1 μm diamond paste. The phase composition of the infiltrated composites was determined by X-ray diffraction. (Rigaku RINT 2100). The residual Si fraction in the composites was determined by analysis of SEM images using the Thixomet[1] software. In order to clarify the morphology of the SiC phase, residual Si was removed by etching the polished samples in 10% HF for 30 s.

2.3. Mechanical properties

Hardness was determined using a Buehler microhardness tester with a Vickers indenter under 20 N load. The flexural strength was determined by three-point bending test. The velocities of longitudinal and transverse acoustic waves were determined by the pulse-echo technique using a 5 MHz probe. The elastic modulus was derived from ultrasonic velocity data and the density values of the composites measured by the Archimedes method. Dynamic compression stress–strain curves were obtained by split Hopkinson (Kolsky) pressure bar testing [12]. Quasi-static fracture testing was carried out on a MTS810 servo-hydraulic machine under displacement control. The loading configuration was that of the three-point bend testing. Since all specimens displayed linear elastic behavior up to fracture, the load at fracture was used for calculations of the fracture toughness. Dynamic fracture testing was carried out using the one-point impact configuration, as described in detail in previous publications [13–15]. In order to probe the failure mechanism under dynamic loading, the fracture path (profile) was investigated using nickel-plated specimens, from which mid-thickness longitudinal sections were prepared through the main fracture plane [16].

[1] Image analysis program, developed at the St. Petersburg State Polytechnic University, Department of Steel and Alloys.

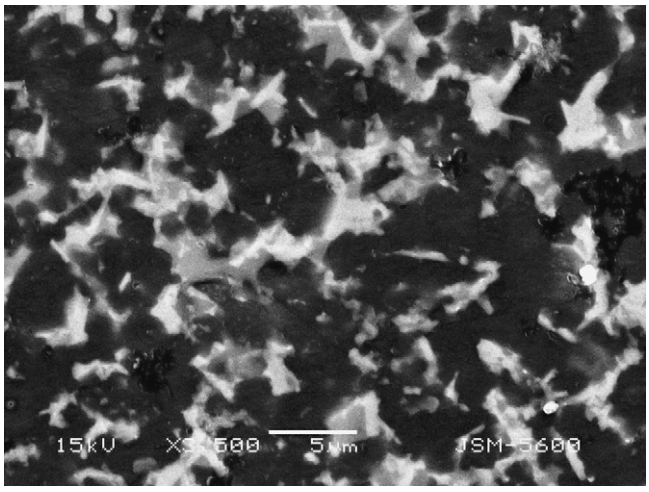

Fig. 1. SEM image of the infiltrated composite, fabricated from the preform with 20 vol.% of porosity.

3. Results and discussion

3.1. Microstructure of the infiltrated composites

The microstructure of the infiltrated B_4C composites (Fig. 1) consists of three phases, namely boron carbide, β-SiC and residual silicon. The β-SiC phase appears as white plate-like particles. The light-gray regions correspond to residual Si, and the dark gray areas are the boron carbide phase. According to the image analysis of the microstructure, the SiC phase constitutes about 13 and 17 vol.% and the residual Si 7 and 13 vol.% of samples with an initial porosity of 20 and 30 vol.%, respectively. The microstructure after etching and removal of the residual silicon (Fig. 2) puts in relief the plate-like SiC phase, in some instances still connected to the original boron carbide particles. The mechanism of the reaction between liquid Si and boron carbide has been discussed previously [5].

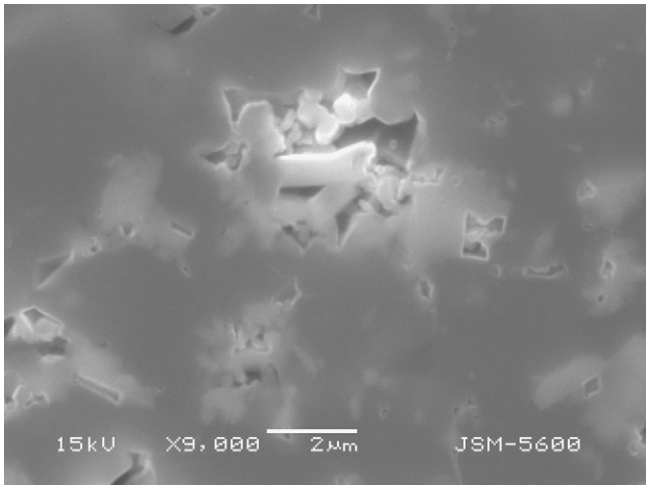

Fig. 2. SEM image of the etched sample. The morphology of the SiC phase is clearly apparent.

Table 1
Static properties of the infiltrated composites

Materials	Density (g/cm^3)	Poisson's ratio	E (GPa)	Hardness (GPa)	Flexural strength (MPa)	K_{1C} (MPa m$^{0.5}$)	Residual Si (vol.%)
S20	2.582 ± 0.060	0.188 ± 0.004	410 ± 9	22.5 ± 1.4	390 ± 70	5.5 ± 2.2	7.0
S30	2.606 ± 0.012	0.189 ± 0.007	370 ± 4	20.3 ± 2.5	415 ± 50	7.9 ± 2.2	13.0

3.2. Static mechanical properties

The values of density, Young's modulus, hardness and flexural strength of the infiltrated composites are presented in Table 1. The two composites display relatively high hardness and Young's modulus values. Both the Young's modulus and the hardness increase, while the flexural strength and K_{1C} decrease with decreasing amounts of residual silicon. The high Young's modulus and hardness values are related to an increased fraction of the ceramic phases within the composites.

In the course of the reaction between liquid Si and the boron carbide preform devoid of free carbon, a plate-like SiC phase with a high aspect ratio is formed [5]. A strengthening effect of these plate-like SiC particles on ceramic composites was reported in Refs. [17,18]. The SiC particle fraction in the S20 samples is lower (13 vol.%) than in the S30 samples (17 vol.%) providing a clue for the increased flexural strength and fracture toughness values in the latter.

3.3. Dynamic mechanical properties

Since the investigated material is relatively hard and brittle, a preliminary stage that leads to a valid stress–strain curve is to assess the dynamic equilibrium of the specimen. Fig. 3 shows the two forces acting on the specimen, from the incident (F_in) and the transmitted (F_out) side of specimen 5 (Table 2). The two forces are quite similar, almost from the onset of the tests, indicating that the specimen is in dynamic equilibrium. This condition was ascertained for each specimen, the mechanical properties of which are reported here. The excellent dynamic equilibrium shows that the Hopkinson bar test can be performed in its classical form, without the need to resort to additional techniques such as pulse-shaping.

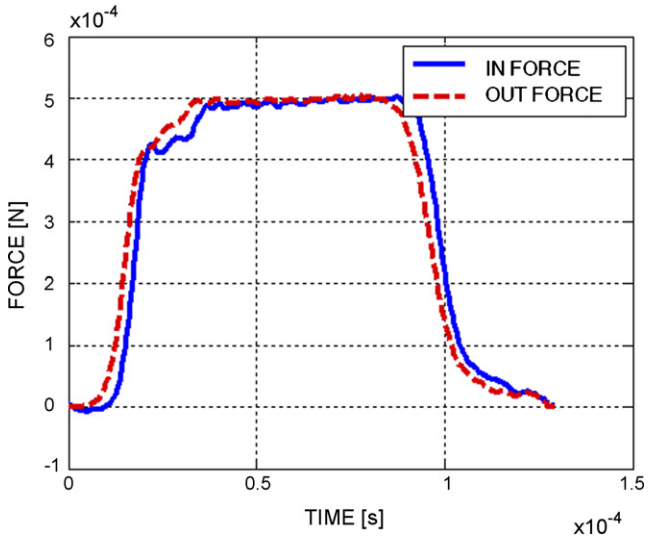

Fig. 3. The two forces that act on the specimen, from the incident (F_in) and the transmitted (F_out) side of specimen 5.

The dynamic (initiation) fracture toughness was tested using the one-point impact configuration. The specimen was in contact with an instrumented (Hopkinson) bar. On the specimen, two fracture gauges are cemented on each side of a sharp notch (in this case). The load applied to the specimen was recorded using the instrumented bar and the (mode I) stress intensity factor was calculated from the onset of the loading process until the crack starts to propagate (fracture), as indicated by the fracture gauges. At this time, the calculated stress intensity factor is interpreted

Table 2
Dynamic mechanical properties of the infiltrated composites

Material	Diameter (mm)	Height (mm)	σ_{max} (MPa)	$\dot{\varepsilon}$, (s^{-1})	Energy (MJ/m^3)
S20 composites					
1	7.04	3.37	1070	2250	18
2	6.98	3.35	1260	5000	30
3	6.97	3.36	1280	3700	30
4	6.83	3.36	1330	3100	35
5	7.02	3.36	1290	2850	21
6	6.97	3.34	1320	2820	30
S30 composites					
1	7.09	3.99	1430	2300	26
2	6.78	3.98	1080	1850	17
3	6.81	3.98	1100	1882	17
4	7.29	4.00	909	1715	12
5	7.15	3.96	1030	2116	17
6	7.14	3.97	1090	1829	13
7	7.04	3.96	1170	1987	19

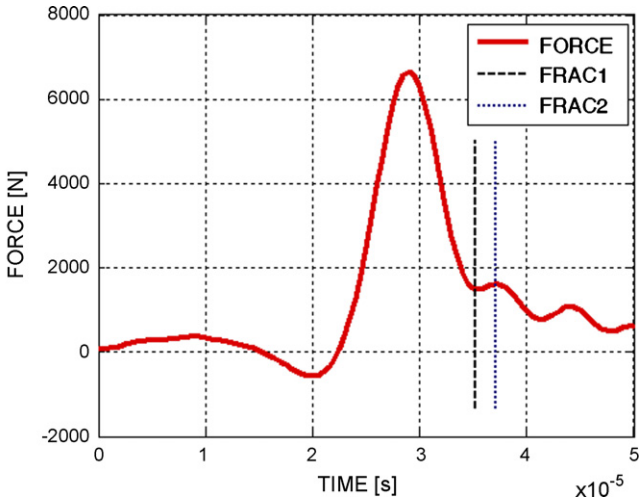

Fig. 4. A typical record of a load–time curve along with the indications of the fracture gauges. It is observed that fracture occurs significantly after the peak-load, which is characteristic of this kind of test.

as the dynamic fracture toughness of the material. Two values were usually measured, one on each side of the specimen, and the test was considered as valid when these two values were sufficiently close (within 15%), and after visual assessment that the crack path was flat and not slanted, which would indicate a mixed-mode fracture. A typical record of a load–time curve is shown in Fig. 4 along with the indications of the fracture gauges. The fracture occurred significantly after the peak-load, which is characteristic of this kind of test.

Typical dynamic stress–strain curves are shown in Fig. 5 the stress–strain curves suggest that the overall ductility to failure is not sensitive to the composition variation within the samples that were examined. The curves are mostly smooth but some oscillations appear before failure. These oscillations are probably related to the failure mechanism, which we believe is associated with the nucleation and coalescence of microcracks [19]. The peak stress is taken as the characteristic dynamic failure stress of the composite.

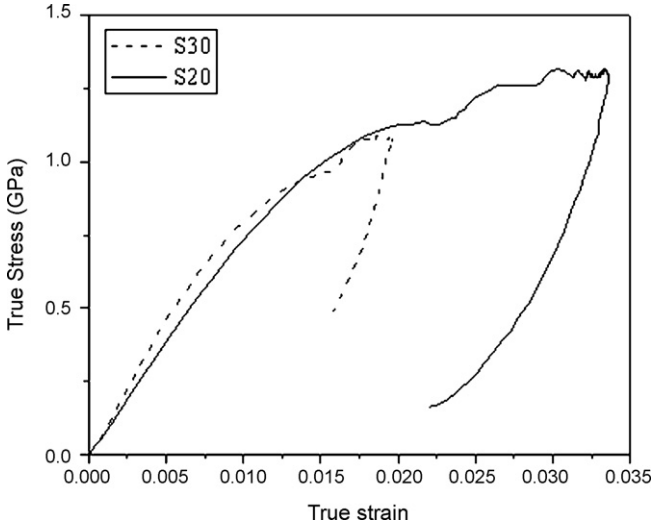

Fig. 5. Typical dynamic stress–strain curves.

Fig. 6. Typical SEM image of quasi-statically fractured specimens.

The dynamic properties of the composites were determined in the 1700–5000 s^{-1} strain-rate range (Table 2). The average values of σ_{max} were 1258 ± 95 and 1118 ± 138 MPa for the S20 and S30 samples, respectively. The experimental results indicate that the infiltrated composites do not appear to be strain-rate sensitive. A similar behavior of the B_4C–Al composites has been reported by Palfey et al. [11], but the compressive fracture strength (σ_{max}) of these composites has been reported to be higher (3800 and 2000 MPa for 80% B_4C–Al and 65% B_4C–Al composites, respectively). This difference is to be attributed to the extended plasticity of the aluminum-containing composites in contrast to the overwhelmingly brittle behavior of the silicon-containing composite.

The measured values of the dynamic fracture toughness (K_{1D}) were 42.6 ± 17.6 and 117.8 ± 28.9 for the S20 and S30 samples, respectively. These values are significantly higher than the K_{1C} values, measured under static conditions. For brittle materials, this finding is not surprising and it may result from specific dynamic crack initiation mechanisms that do not operate at quasi-static rates, as shown in Ref. [16]. Although, the dynamic fracture toughness (K_{1d}) of the S30 composites is

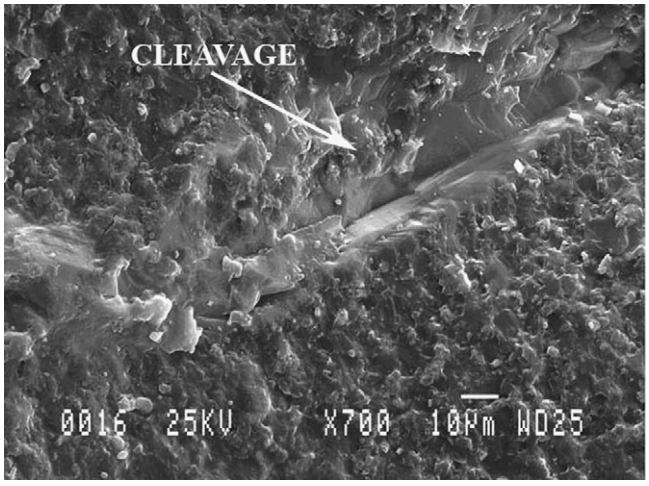

Fig. 7. Typical SEM image of dynamically fractured specimens.

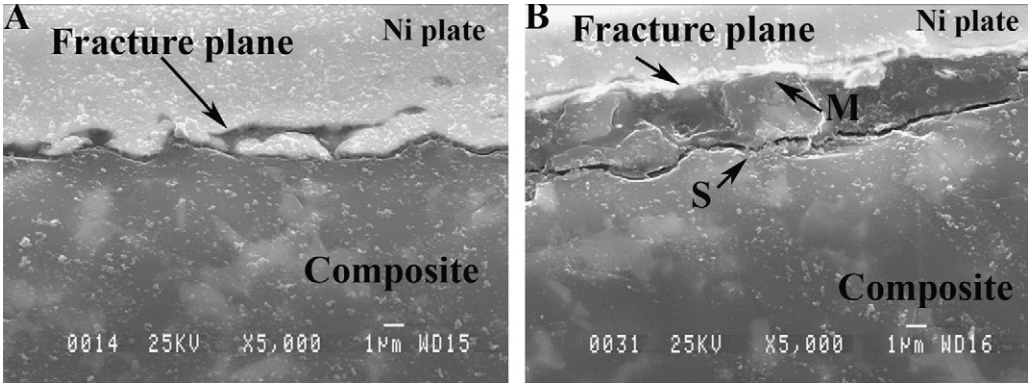

Fig. 8. Typical fracture path (profile) of samples after quasi-static (A) and dynamic (B) failure.

higher than that of the S20 composites, the average value of the energy absorption up to failure for the S30 composites, is 17.2 MJ/m^3 while for the S20 composites it is significantly higher (27.3 MJ/m^3). The values of the dynamic fracture toughness reflect a crack initiation process, whereas the values of the energy absorption are related to the overall failure process, including dynamic crack propagation. Thus, these two toughness values provide an overall picture of the dynamic fracture behavior of the composite.

3.4. Failure mechanisms

Typical fracture surfaces of specimens after quasi-static and dynamic loading are shown in Fig. 6 and Fig. 7, respectively. In both cases the operation of cleavage-like fracture mechanisms was clearly detected. The static fracture takes place only along one plane and may be attributed to the critical crack propagation (Fig. 8A), while the dynamic fracture occurs along several distinct planes, in which a secondary set of cracks, denoted S, appears to run parallel to the main fracture plane (M) (Fig. 8B).

4. Conclusion

Boron carbide composites with a reduced fraction of residual silicon have relatively high values of hardness and Young's modulus, but their flexural strength and fracture toughness decrease with decreasing residual silicon. In the sample with higher initial porosity, a larger fraction of plate-like SiC was generated leading to increased flexural strength and fracture toughness on account of the strengthening effect of the high aspect ratio of the second ceramic phase particles. The dynamic strength and the dynamic fracture toughness K_{1d} are significantly higher than the corresponding static properties and are insensitive to the residual silicon fraction and to the strain-rate (up to $\dot{\varepsilon} = 10^3\ s^{-1}$).

Acknowledgment

This work was partly supported by the Israel Science Foundation grant 118/03.

References

[1] F. Thévenot, J. Eur. Ceram. Soc. 6 (1990) 205–225.
[2] P. Popper, In Special Ceramics 1., British Ceramic Research Association, London, 1960, pp. 209–219.
[3] K.M. Taylor, R.J. Palicke, U.S. Patent No. 3,765,300 (1973).
[4] M.K. Aghajanian, B.N. Morgan, J.R. Singh, J. Mears, R.A. Wolffe, in: J.W. McCauley, et al. (Eds.), Ceramic Armor by Design, The American Ceramics Society, Westerville, OH, 2002, pp. 527–539.
[5] S. Hayun, N. Frage, M.P. Dariel, J. Solid State Chem. 179 (9) (2006) 2875–2879.
[6] D.P. Dandekar, Report No. ARL-TR-2456 (2001).
[7] C. Mingwei, J.W. McCauley, J.K. Hemker, Science 299 (5612) (2003) 1563–1566.
[8] T.J. Vogler, W.D. Reinhart, L.C. Chabildas, J. Appl. Phys. 95 (8) (2004) 4173–4183.
[9] D.E. Grady, SAND 94-3266, Sandia National Laboratories (1995).
[10] L.C. Chhabildas, W.D. Reinhart, D.P. Dandekar, in: J.W. McCauley, et al. (Eds.), Ceramic Armor Materials by Design, The American Ceramics Society, Westerville, OH, 2002, pp. 269–278.
[11] W.J. Palfey Jr, D.A. Koss, W.R. Blumenthal, First International Conference on Advanced Materials Processing, ICAMP 2000, 2000, pp. 19–23.
[12] H. Kolsky, Stress Waves in Solids, Dover Publications, New York, 1963.
[13] G. Weisbrod, D. Rittel, Int. J. Fract. 104 (1) (2000) 89–103.
[14] D. Rittel, N. Frage, M.P. Dariel, Int. J. Solid Struct. 42 (2) (2005) 697–715.
[15] D. Rittel, A.J. Rosakis, Eng. Fract. Mech. 72 (2005) 1905–1919.
[16] D. Rittel, Int. J. Fract. 106 (2) (2000) L3–L8.
[17] S.K. Lee, Y.C. Kim, C.H. Kim, J. Mater. Sci. 29 (20) (1994) 5321–5326.
[18] W.J. Moberlychan, J.J. Cao, L.C.D.E. Jonghe, Acta Mater. 6 (5) (1998) 1625–1635.
[19] W.D. Kaplan, D. Rittel, M. Lieberthal, N. Frage, M.P. Dariel, Scripta Mater. 51 (1) (2004) 37–41.